Self-regulated symmetric breaking enables full-space phototaxis of animate materials

Guodong Hou[1,2,3,4], Xu Zhang[1], Feihong Du[1,2,3], Yadong Wu[4], Xing Zhang[1], Zhijie Lei[1,2,3], Wei Lu[1,2,3], Feiyu Zhang[1,2,3], Guang Yang[3], Huamiao Wang[1], Zhenyu Liu[4], Jiangping Chen[1,3], Guang Meng[1,2], Nicholas X. Fang[5]*, Xiaoshi Qian[1,2,3]*

[1]State Key Laboratory of Mechanical System and Vibration, Shanghai Jiao Tong University, Shanghai, China.

[2]Interdisciplinary Research Centre for Engineering Science, School of Mechanical Engineering, Shanghai Jiao Tong University, Shanghai, China.

[3]Institute of Refrigeration and Cryogenics, School of Mechanical Engineering, Shanghai Jiao Tong University, Shanghai, China.

[4]Institute of Engineering Thermophysics, School of Mechanical Engineering, Shanghai Jiao Tong University, Shanghai, China.

[5]Department of Mechanical Engineering, The University of Hong Kong, Pokfulam Road, Hong Kong, 999077, China

*To whom correspondence should be addressed. Email: xsqian@sjtu.edu.cn, nicxfang@hku.hk

Abstract

Living organisms in their early forms adopted simple structures and could adapt to different cues from the ambient environment in a highly regulated and efficient manner. However, synthetic systems have achieved less with more human intervention than their natural counterparts. Here, we show that a simple animate material can recognize the directions of constant photonic illumination and follow a path with strong directional regulation inside a constraint-free, fluidic space. By spontaneously breaking the symmetry of multiple surrounding energy fields, the nanostructured stimuli-responsive polymers-based animate material swiftly assumes an optimal pose and creates directional flow around itself, which it follows to achieve robust full-space phototaxis. In addition, this phototaxis enables a series of complex, self-adaptive locomotion underwater. We demonstrate that this versatility is empowered by the fast reconFigurability and synergy of photo-fluidic interactions composing closed-loop self-control. The untethered, ambient-powered animate-material manoeuvres through obstacles agilely, following the cues of constant illumination without any electronics or close-range human intervention.

Planktonic microbes move hundreds of metres towards the surface each night to feed before retreating back down at dawn[1,2]. Many of them have developed receptors for directed locomotion, known as phototaxis, gyrotaxis, rheotaxis, and chemotaxis, so they can sense many ambient gradients and move along a preferred direction to acquire food and the chance for reproduction and move away from danger in an adaptive and sustainable manner[3,4]. This behaviour links the epipelagic and mesopelagic zones, critically contributing to the oceanic biological carbon pump[5,6]. Inspired by nature, recent years have witnessed extensive pioneering efforts to advance robots in a fluidic environment across a great range of scales[7-14]. However, the controls of the artificial systems still rely on preprogramed electronics and a high level of human attention at close range, *i.e.*, magnetic field manipulation[15,16], accurate aiming[10,17], flash frequencies of lasers[8,18], and preset constraints in space[17,19]. These prerequisites and special conditions do not exist in nature and hence set obstacles to practical application.

Breakthroughs have been achieved in self-regulated materials[20,21] for autonomous phototropic tracking[22] and oscillation[17]. The demonstrated photophobic taxis was constrained to a water surface and within a one-dimensional fluidic channel[17]. By far, synthetic systems that are capable of omnidirectional, full-space phototaxis without electronics or human intervention remain a highly desirable goal with the aim to design an embodied cognitive material[23-25] in free space rather than a reflexive material under many limitations.

Here, we develop a monolithic, animate-material system that recognizes and moves in any direction of constant photonic illumination (**Fig. 1**). As shown in **movie S1**, the untethered soft material identifies the direction of irradiation and move towards it, submerged in an aqueous environment. While illuminated, the soft robot harnesses the photonic energy and breaks the symmetry of temperature, flow fields, and morphology. The multi-physical symmetric-breaking allows the animate material to sense the direction of the incidence (**Fig. 1a**), create a phototropic stream that provides propulsion (**Fig. 1b**), and spontaneously assume the optimal posture and gait (**Fig. 1c**) for swift phototactic locomotion.

During the symmetric-breaking-induced locomotion, the animate material is capable of self-regulating the photonic energy-input by adaptively enhancing convective heat loss around itself, which provides negative feedback for the correction of deviated traveling direction (**Fig. 1d, e**) to implement robust phototactic manoeuvres. The material system employs an ultra-high-sensitivity stimuli-responsive material that recovers at an unprecedented rate to allow a fast response to any new event (**Fig. 1f**), offering a steering finesse of full-space phototaxis that is completely based on the cognition of the material itself (**Fig. 1g**).

Spontaneous symmetric breaking and recovery

We adopt a simple geometry similar to a jellyfish with axial symmetry that comprises a hemispherical bell and six vertical tentacles. The monolithic structure of the jellyfish-like phototactic vehicle (JPV) permits facile additive manufacturing technology, such as PμSL, as well as moulding manufacturing for mass production (**Supplementary Fig. S3**). The bell contains an air bubble as a key component for balancing gravity and breaking the symmetry of the density distribution (**Fig. 1c**). Without directional illumination, the bubble is kept in an up-centre position, providing buoyancy to partially balance gravity and keeping the JPV in an upright position.

The universal design of JPVs can be fulfilled with many active materials, *i.e.*, light-active polymers[26-28] and electroactive polymers[29-32]. Here, we select the stimuli-responsive poly(N-isopropylacrylamide) (PNIPAAM)-based hydrogel[33] as an example for its iconic, reconFigurable morphing across its low critical solution temperature (LCST). Similar to the sensory system spread all over the body of a squid[34], the hydrogel is homogeneously blended with highly efficient photo-thermal nanoparticles, such as Au nanoparticles (AuNPs) and reduced graphene oxides (r-GO), to ensure omnidirectional sensing of incident photons[35] (**Supplementary information Section 1**).

Once illuminated, three symmetries of the JPV are broken simultaneously: 1. a temperature gradient is established along the direction of the illumination, due to the effective photothermal coupling that heats the illuminated surface (**Fig. 2a and Supplementary Fig. S7)**; 2. a convective flow field is generated from the heated surface (**Fig. 2b**); 3. when the local temperature is higher than the LCST, the local shrinkage of the gel squeezes the embedded bubble balancer away from its symmetric position in the bell (**Fig 1c, 2c** and **Supplementary Video 2**), introducing a redistribution of density and hence a phototropic tilting towards the light source (**Fig. 2d**). The phototropic behaviour was not observed in the control sample made of thermally inactive poly(acrylamide) (**Supplementary Fig. S12**) with the same amount of photo absorbers. We employ a multi-physics model based on the finite element method (FEM) to investigate the synergy of the multi-energy coupling that governs symmetric breakings (**Supplementary Fig. S7**). The mechanical strain and temperature gradient showed great agreement with the experimental results (**Fig. 2a, d**). As shown in **Fig. 2d**, the off-centred bubble leads to a rapid rearrangement of the JPV's centre of buoyancy (B), causing the metacentre (M) to move below the centre of gravity (O), generating a clockwise torque under illumination from the right. The torque exhibits a self-adaptive lean towards the direction of illumination, offering reduced fluidic drag that favours phototaxis (**Supplementary Fig. S20c**), as the JPV identifies the direction of the incidence and prepares itself for movement. Our theoretical analysis shows that the drag coefficient is reduced by 30% when the tilting angle changes from 90° (upright position) to 50° (**Supplementary Fig. S20**).

Agile phototactic behaviour demands ultrafast recovery to prevent a time lag resulting from a varying direction of illumination (**Fig. 2e**). However, the re-swelling rate of PNIPAAM-based hydrogels is notoriously slower than their shrinking rate. To restore the chronic symmetry of actuation and recovery, we modify the porous size and porosity of the gel by tightly controlling the chemical and physical processes of fabrication. For quantitative analysis, we tested the rate of phototropic actuation and recovery of the tentacle for different angles of incidence. At an angle of 20°, the ice-templated, hybrid-crosslinked hydrogel pillar fully recovers less than a second, which is 30 times faster than the best previously reported values[34], under similar pre-conditions (**Fig. 2f, g**, and **Supplementary Information Section 2**).

Photothermal-tactic flow

Planktonic organisms, ranging from bacteria to jellyfish, move around by following the flows, waving or rotating their flagella or lappet, mostly at a low Reynolds number. The JPV is designed to harness the momentum from the ambient light that translate into photothermal-tactic flows. Their tentacles provide functions such as balance keeping and grabbing, rather than providing propulsion. In nature, propulsion efficiency at low Reynolds numbers is low (~1%–3%)[36], fundamentally because the thrust is generated by the same mechanism that resists motion: viscous drag. On the other hand, plankton are capable of moving hundreds of metres by adaptively positioning themselves in a favourable current. Hence, generating photothermal tactic flow around the JPV (mostly a passive element) is an important task for achieving long-distance, underwater phototaxis.

In the JPV, the momentum is originated from the temperature gradient, which defines the direction of the photothermal flow. Maintaining the symmetric-broken temperature field requires synergy between the photo-thermal environment inside and around the JPV, *e.g.*, the thermal conductivity, photonic penetration length, convection, and characteristic size, *etc*. Therefore, we studied Biot number of the JPV. As most plankons, JPV contains majorly water holding inside polymer chains. The skin of the JPV exhibits high absorption hence the illuminated surface can be treated as a surface heat source. We find that the photothermal-tactic flow induced acceleration of the JPV is scaling insensitive (**Supplementary Fig. S22**) as long as the JPV is larger than a critical size (1 mm in current design) that is capable of maintaining effective symmetry breaking (**Supplementary Fig. S24**). The observation is consistent with the analysis of size-dependent Biot number (*Bi*). Further reducing thermal conductivity of the JPV body could extend the critical size down to the scale of tens of micrometres (**Fig. 2h**).

As schematically shown in **Fig. 2i**, when illuminated from the above, the JPV quickly ascends to the surface (**Fig. 2j**), reminding us of the vertical migration of marine plankton that represents the largest biomass transport on Earth[37]. Homogeneously distributed photo-thermal nanoparticles efficiently transduce photonic energy from all directions to thermal energy[38]. The elevated temperature on the illuminated surface creates a convective flow indicating directional information (**Fig. 2k**). To examine the hydrodynamic details, we conducted particle image velocimetry (PIV) to monitor the flow field that carries the JPV. The results are in good agreement with FEM-based computational fluid dynamics (CFD) simulation (**Fig. 2k, l**).

The PIV images of the hydrodynamic footprint reveal that the velocity distribution of the surrounding fluid moves as the JPV moves (**Fig. 2m and Supplementary Video 3**). We observe vortices during the phototactic movement of the JPV, which is considered a sign of inertial swimming[10]. The convective flow occurring around the JPV can be recognized as laminar flow based on the Reynolds number $Re=uD/v$ (where u refers to the gliding velocity, D is the characteristic size, and v is the kinematic viscosity of the water). The PIV data indicate that the JPV is swimming in the low-Reynolds-number region where its natural counterparts live. During vertical ascendance, the submerged JPV is subjected to gravitational force G, buoyancy force F_B, drag force F_D, and lift force F_L, and this upwards locomotion away from the bottom occurs as long as $F_B+F_L>F_D+G$ (**Supplementary Fig. S22**). Vertical phototaxis is intensity-cognitive (**Supplementary Video 4 and 5**). The JPV can sense the power density of the photo-illumination, lean, and steer towards the brighter zone when the light field is not evenly distributed in space (**Supplementary Fig. S15 and Video 5 demo1**).

The intensity cognition is attributed to the synergy of multiple energy interactions, including photothermal energy transduction, thermochemical phase transition, chemo-mechanical deformation, thermofluidic convection flow, and flow–soft matter interaction. The synergy allows the JPV to maintain exposure and lean towards the brightest irradiation, which results in a high velocity of phototactic movement (**Supplementary Fig. S14a-d**). Constrained by the size of the container, the highest speed of the JPV is 18 mm/s and 1.5 BLs/s (**Supplementary Fig. S14d and Video 4**), which is significantly higher than those of many electric powered and tethered underwater robotics (**Supplementary Fig. S14e and table S1**) and comparable to those of many mammalian and non-mammalian organisms in nature that typically move at speeds exceeding 1 BL/s[39].

Compared to vertical phototaxis, phototaxis along any other direction (**Fig. 2n**) is more complicated to achieve due to temperature-induced upwelling. Under horizontal irradiation from the right, the symmetry of the temperature and flow field are broken, producing higher temperature and fluid velocity on the illuminated side (**Fig. 2o**). The temperature gradient near the illuminated surface reflects the directional information of the incidence but is also coupled with the adjacent flow field (**Fig. 2p**). The CFD and PIV results (**Fig. 2q, r**) indicate that the flow field consists of a significant part of the upwards convective flow that carries the JPV upwards and to the right (**Fig. 2r**), resulting in inaccurate horizontal phototaxis. Additional measures should be taken for the JPV to self-regulate the upward flow, *e.g.*, reducing its surface temperature on-demand as negative feedback[20], in order to continuously move in the direction of illumination.

Directional self-regulation

As the major provider of the fluidic thrust, the temperature gradient near the illuminated surface is defined by the input photonic heating power and the cooling power output to the ambient. We present two mechanisms to regulate the local temperature, hence enabling the locomotion of the JPV by allowing the JPV to self-manipulate the ambient convective heat transfer during movement.

Successful horizontal phototaxis is achieved, as shown in **Fig. 33a** and **Supplementary Video 1**. Under 532-nm laser irradiation, the AuNP-incorporated JPV automatically leaps up and forwards and falls back to the bottom. During each jumping cycle, only the horizontal displacement accumulates via phototaxis. The hopping cycle can be initiated under irradiation lower than 1000 W/m^2 (**Supplementary Fig. S28a, b**). To further investigate the self-regulatory behaviour, we simulated and monitored the speed and the surface temperature of the JPV in situ during the phototactic hopping cycles. The *in-situ* monitored correlation between the speed and the local temperature of the JPV is in good agreement with the CFD simulation (**Supplementary Fig. S28c, d**). The speed and temperature-correlated convective heat transfer coefficient can be obtained as the mixed Nusselt number ($Nu=(Nu_n^4+Nu_f^4)^{1/4}$)[40,41], where Nu_n is the natural convection and is related to the Rayleigh number (*Ra*), and Nu_f refers to forced convection that is determined by the Reynolds number (*Re*) (**Supplementary Information Section 3.2**).

To study the multi-physical, photo-thermo-fluidic dynamics, we show the time evolutions of scalar quantity of speed (v), local temperature (T), convective heat transfer coefficient (h), input photonic power (P) and convective cooling power (q) near the illuminated bell area for two consecutive hopping cycles. When the JPV is ascending and subsequently moving away from the laser, the temperature saturates, and the speed of the JPV drops to zero, indicating strong photonic regulation. After a short period of inertial ascendance, the JPV falls back and completes the negative feedback cycle. The self-avoidance of light incidence indicates a strong photo-thermal regulation, which is quite similar to the characteristic thermal dance of shovel-snouted lizards (*Meroles anchietae*) to avoid overheating of their feet.

Notably, the ascending JPV exposes its photo-responsive tentacles to the laser beam and aligns with the incidence automatically (**Fig. 3a, b**) as the JPV controls its direction of movement. The bent tentacle strengthens the leaning pose, which helps protect against upwards flow, facilitate horizontal motion.

Compared to the narrow laser beam, which requires constant human involvement to keep aiming at the JPV, phototaxis towards a wide beam-width incidence may represent a more general case in the natural environment. The challenge is to achieve thermal regulation when the JPV can no longer hide from the light. Surprisingly, we observe similar hopping cycles (**Fig. 3c**) of the JPV illuminated by a spotlight. The speed and thermal analysis (**Fig. 3d**) show that the JPV is diving at a faster speed (2.5-fold) than that corresponding to laser illumination with the same total energy (**Supplementary Fig. S9**). The enhanced speed can be attributed to the continuous illumination of the spotlight that accumulates more momentum than in the case of self-avoiding-induced intermittent illumination. The high-speed JPV encounters ambient cold fluid more rapidly, in **Fig. 3d**, we show that the time-dependent h is strongly correlated with the time evolution of the real-time speed, suggesting speed-induced thermal regulation. Nusselt number corresponding to the maximum velocity of photonic and thermal regulation are comparable, however, the Richardson number ($Ri=Gr/Re^2$, representing the importance of natural convection relative to forced convection, where Gr is Grashof number and Re is Reynolds number) of photonic regulation is more than 20 times higher than that of thermal regulation, indicating that they are dominated by natural and joint convection, respectively (**Fig. 3e**). The much-increased convective heat transfer ($hA\left(T_s - T_f\right)$) regulates the surface temperature and fulfils a negative feedback loop (**Fig. 3f**). By utilizing effective thermal regulation, full-space and omnidirectional phototaxis is achieved for any 3-D incident angle (**Supplementary Fig. S29 and Video 1 demo2**).

In addition, the JPV offers various hopping frequencies for selection by manipulating its excess gravity against the input photonic power. By reducing the volume of the bubble in the bell, the hopping frequency continues to decrease until an extreme case is reached in which the JPV slides horizontally instead of hopping (**Supplementary Fig. S31** and **Video 6**). The tuning of the excess gravity is an effective tool to preset the phototactic behaviour according to the different ambient light, thermal and fluidic conditions in practical field deployment.

Demonstration of complex locomotion

The highly regulated phototaxis of the JPV can be characterized by the distance of the accurate tracking and the angular resolution. Distinguished from acquiring momentum from paddling a single tentacle that can be easily misaligned with the laser beam, the JPV performs robust phototaxis over a long distance without directional deviation (**Fig. 4a, b and Supplementary Fig. S33**). Limited by the dimension of the experimental space, the JPV exhibits accurate phototaxis of 300 mm compared to 4.3 mm for single-tentacle paddling. In addition, by carefully cascading the strokes by 6 off-centre-positioned tentacles, the JPV adapts to exhibit rotational advance (**Fig. 4c and Supplementary Video 7**). The bent tentacle counteracts the overturning moment and hence provides additional balance when the JPV is climbing a ramp, further ensuring the stability of the movement (**Fig. 4d and Supplementary Video 8**)). These tentacles can also serve as photonic or thermal sensitive grabbers that can track and grasp a bright or hot object (**Supplementary Fig. S13**).

Due to the spontaneous symmetric breaking and fast recovery of the polymeric matrix (**Fig. 1g**), the directional response of the JPV is instant. We observe that the JPV is capable of agile manoeuvring with fine directional and positional resolution. Following a constant light source with continuously varying angles, the JPV travels perfectly along with the complex strokes of Chinese calligraphic characters “自然” (**Fig. 4e and Supplementary Video 9**), which means “nature” and is written in the cursive script style (with connected characters). In addition to the capability of fine steering, we further demonstrate long-distance operation of the JPV with a beam-expanded laser placed 10 m away (**Supplementary Fig. S18**).

Different from the phototropic taxis when submerged, the JPV shies away from the light once it is floating on the water–air interface (**Fig. 4f**). The photophobic behaviour is induced by Marangoni convection, which is attributed to the symmetric breaking of surface tension on the bell at the water surface. Both phototactic modes are capable of accurately following the paths of the character “SJTU” (**Supplementary Fig. S32c, d)**

Combining the two phototactic behaviours, the JPV can dive up to the water surface and move away from the light to avoid obstacles (**Supplementary Fig. S33 and Video 10**) and then dive back in and move towards the light (**Supplementary Video 11**). The cyclic behaviour is similar to the diurnal vertical migration and cycling of many planktonic biomasses and may offer a synthetic platform to mimic the oceanic carbon cycle. For practical field operation, the JPV can be scaled facilely and serve as a phototactic vehicle carrying other functional parts and electronic devices if necessary. For example, we demonstrate self-supported cycling in a series of microalgae-incorporated JPVs (**Supplementary Fig. S34 and Video 12**), in which the microalgae serves as the photothermal converter and can provide many biological and ecological functions. The animate-material system is also capable of sustainable cycling in a swarm, churning the ambient fluid under the cue of a constant spotlight (**Supplementary Fig. S35 and Video 13**).

Acknowledgements: This work was supported by National Key R&D Program of China (2020YFA0711500), and National Natural Science Foundation of China (52076127), Natural Science Foundation of Shanghai (20ZR1471700, 22JC1401800), X.Q. thanks the support by the State Key Laboratory of Mechanical System and Vibration (Grant No. MSVZD202211), the Oceanic Interdisciplinary Program of Shanghai Jiao Tong University (project number SL2020MS009), the Prospective Research Program at Shanghai Jiao Tong University (19X160010008), the Thousand Talent Young Scholar Program, the Student Innovation Center and the Instrumental Analysis Center at Shanghai Jiao Tong University. N.X.F. acknowledges the startup funding provided by the Global STEM professorship scheme sponsored by the Government of the Hong Kong Special Administrative Region.

Author contributions: X.Q. conceived the concept, designed the experiment, and wrote the manuscript. X.Q., G.H. Z.L., F.D., W.L. carried out the material synthesis, characterization and systematic demonstration. G.H., Y.W., G.Y, X.Q., N.X.F. conducted the fluid dynamic experiment and analysis. G.H., X.Z, H.W., X.Q., carried out the numerical simulation. J.C, and G.M. supervised the device modeling. X.Q., and N.X.F supervised the project. All authors analysed and interpreted the data.

Author Information: Reprints and permissions information is available at www.nature.com/reprints. X.Q. is applying for patents related to the described work. The other authors declare no competing financial interests. Correspondence and requests for materials should be addressed to X.Q. (e-mail: xsqian@sjtu.edu.cn).

Supplementary Information is available in the online version of this paper at www.nature.com/.

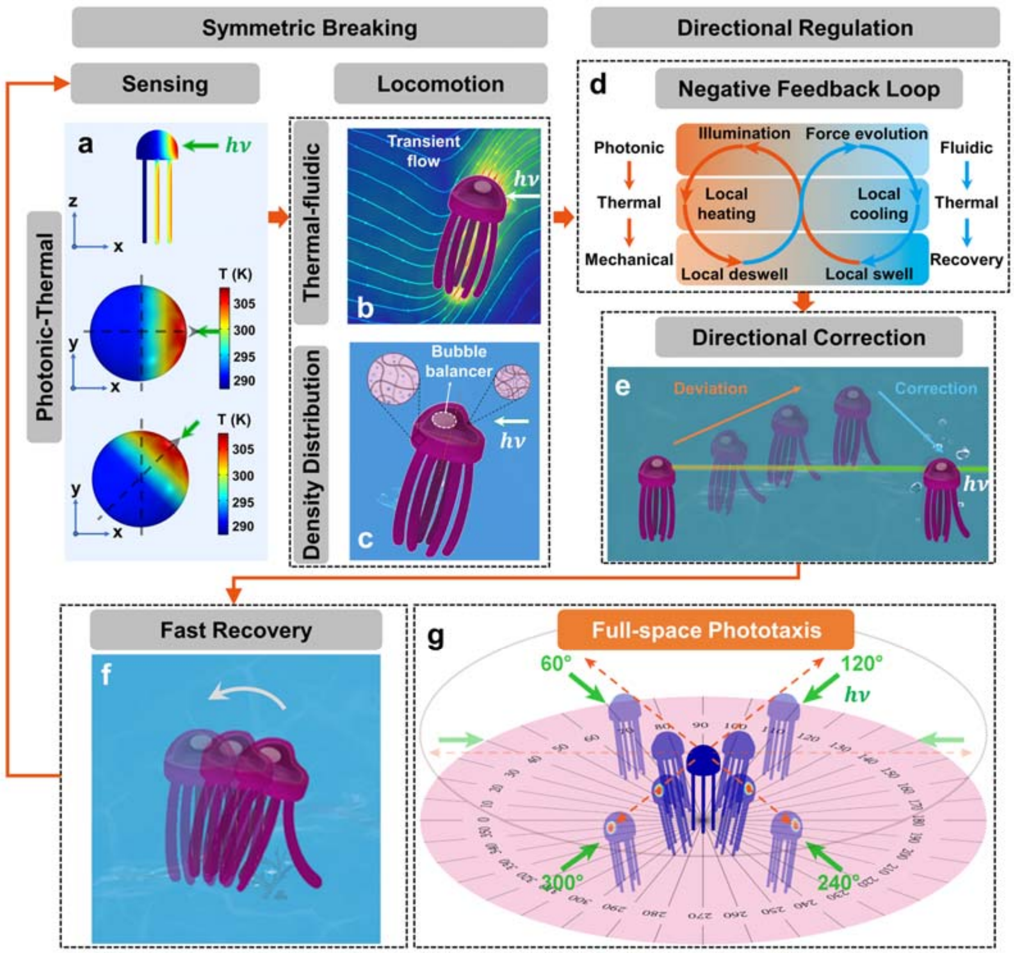

Fig. 1. Schematics of full-space phototaxis enabled by regulated symmetry-breaking. a, Simulated temperature gradient of the illuminated animate-material, due to the photo-thermal coupling. The symmetry-breaking of temperature allows the material to sense, recognize and move along the direction of photonic incidence. $h\nu$ refers to the photonic incidence, $\vec{v}$ the vector of temperature gradient and moving direction. **b, c**, Schematics of the thermally induced fluidic field (b) and thermo-mechanical coupling induced density redistribution (c), both are the results of the symmetric breaking. **d**, Schematics of self-regulated locomotion that enables a negative feedback loops and resulting **e**, Directional correction by the material itself. **f**, Schematics of the fast recovery of the animate material system that is a key that enables the fast response to the instantly changing direction of illumination. **g,** Schematic of the full-space phototaxis.

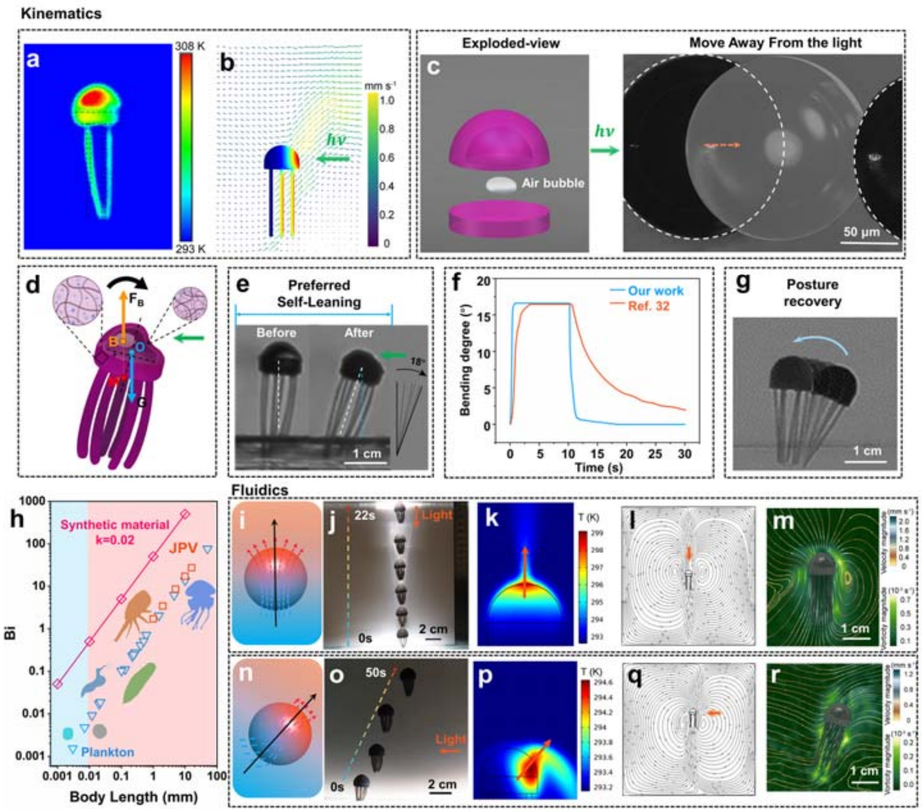

Fig. 2. Photothermal-tactic flow-guided movement. **a**, Infrared image of the JPV under photonic irradiation. **b**, Snapshot of a PIV image showing the broken symmetry of the flow field, in which the JPV model is included to highlight the location in the PIV experiment and the temperature gradient. **c**, Schematic exploded-view and photographic image of the embedded bubble of the JPV. The bubble in the bell moves away from the irradiation from the left. **d**, Local shrinkage squeezes the bubble and deviates the center of force to produce overturning moment. **e**, Self-leaning effect of 18° due to symmetric breaking induced by the relocation of the bubble. **f**, Actuation and recovery rate (for 20° bending) of the ultrafast hydrogel designed for the JPV and comparison with previously reported data. **g**, Posture recovery when the symmetries of the JPV are restored. **h**, Comparison of Biot number of plankton, synthetic material and JPV. **i**, Schematic illustration of vertical illumination, where the heating of the top brings about an upward fluid motion. The arrows indicate the direction of the photothermal tactic flow. **j**, Composite image showing the JPV ascending from the bottom to the water surface under vertical illumination. **k, l**, FEM-simulated temperature gradient (**k**) and flow field (**l**) around the JPV under vertical illumination. **m**, Magnitude of velocity and vorticity recorded by PIV flow measurement during vertical illumination. **n**, Schematic illustration of asymmetric illumination, where local heating generates asymmetric fluid motion. The arrows indicate the direction of photothermal tactic flow. **o**, Composite image showing the movement of the JPV under horizontal illumination. **p, q**, FEM-simulated temperature gradient (**p**) and flow field (**q**) around the JPV under horizontal illumination. **r**, Magnitude of velocity and vorticity recorded by PIV flow measurement during horizontal illumination. Input photonic power density: 2 mW • mm^{-2}.

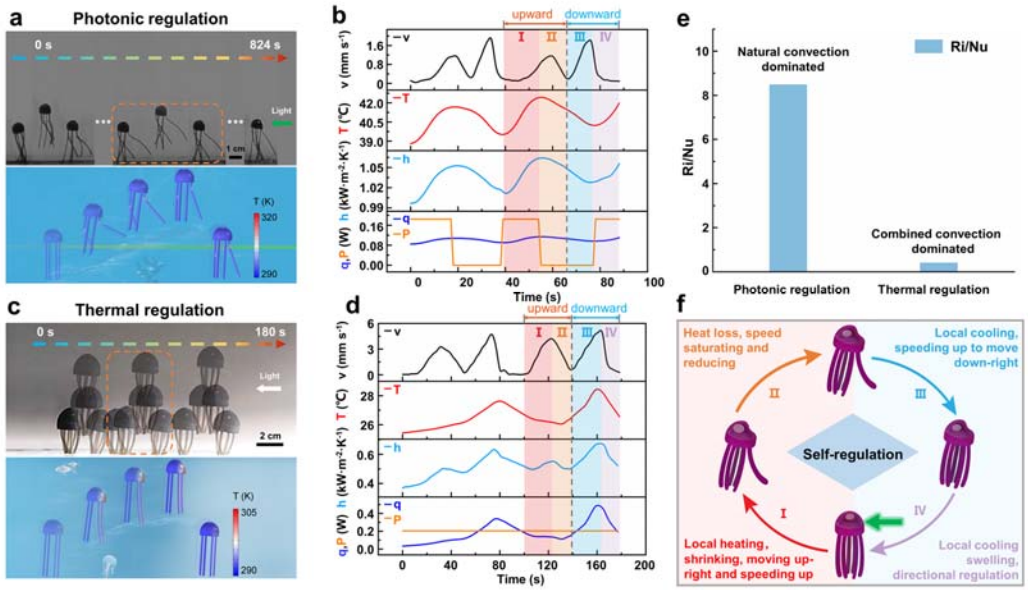

Fig. 3. Phototaxis of the JPV enabled by self-regulated symmetric breaking. a, Composite snapshots and FEM analysis of phototactic hopping towards a laser source (532 nm, 200 mW) **b**, Time evolutions of scalar velocity, temperature, convective heat transfer coefficient, input photonic power and convective cooling power near the illuminated bell area of the JPV over two consecutive cycles. **c**, Composite snapshots and FEM analysis of phototactic hopping of the JPV towards a spotlight (beam diameter of 10 cm, 2 mW • mm^{-2}). **d**, Time evolutions of scalar velocity, temperature, convective heat transfer coefficient, input photonic power and convective cooling power near the illuminated bell area of the JPV over consecutive cycles. **e**, Comparison of Richardson number and Nusselt number for photonic and thermal regulation when velocity is at its peak. **f**, Summarized mechanism of the phototactic locomotion. The JPV’s motion automatically introduces negative feedback loops that regulate photonic and thermal-energy-induced symmetric breaking.

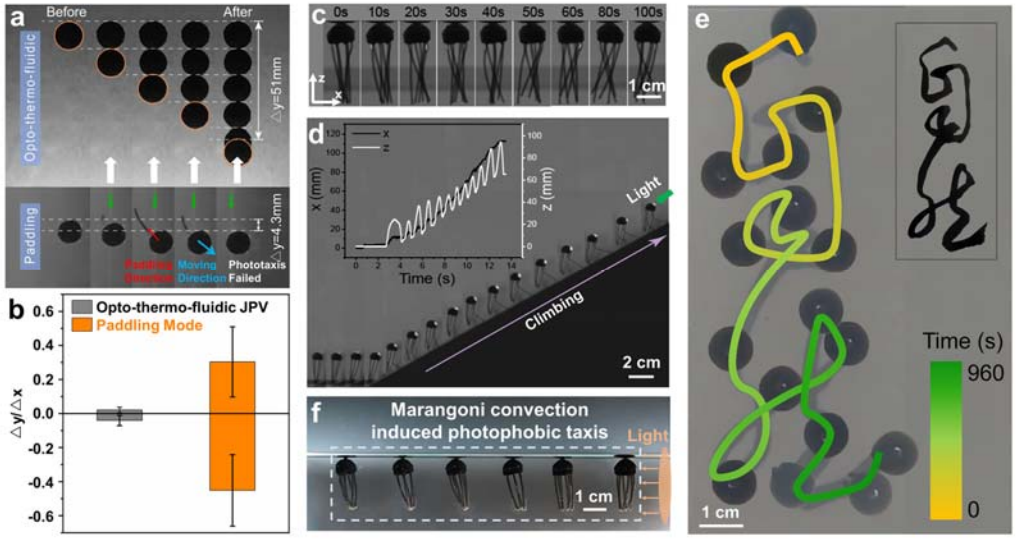

Fig. 4. Accurate and sophisticated motions of underwater phototactic steering. a, Comparison of the phototaxis accuracy in the photo-thermal-fluidic mode (top) and tentacle-paddling mode (bottom). The former achieves travel over at least 51 mm (limited by the size of the container), whereas the latter exhibits a failure to move after 4.3 mm due to misalignment between the tentacle and the laser beam. **b**, Analysis of phototactic accuracy by quantifying the deviated displacement along the y-axis over the travelling distance in the x direction (△y/△x). **c**, Snapshots showing the rotational advancing of the JPV by cascading the strokes of different tentacles. **d**, Composite snapshots and trajectory curve (inset) depicting the phototactic climbing of the JPV in x and z directions. **e**, JPV manoeuvred with finesse, accurately representing each stroke of the Chinese calligraphic characters "自然". **f**, At the water surface, the JPV shies away from the light due to Marangoni convection.

References

1. Stich, H.-B. & Lampert, W. Predator evasion as an explanation of diurnal vertical migration by zooplankton. *Nature* **293**, 396-398 (1981).
2. Behrenfeld, M. J. *et al.* Global satellite-observed daily vertical migrations of ocean animals. *Nature* **576**, 257-261 (2019).
3. Guasto, J. S., Rusconi, R. & Stocker, R. Fluid mechanics of planktonic microorganisms. *Annual Review of Fluid Mechanics* **44**, 373-400 (2012).
4. Oteiza, P., Odstrcil, I., Lauder, G., Portugues, R. & Engert, F. A novel mechanism for mechanosensory-based rheotaxis in larval zebrafish. *Nature* **547**, 445-448, doi:10.1038/nature23014 (2017).
5. Boscolo-Galazzo, F. *et al.* Temperature controls carbon cycling and biological evolution in the ocean twilight zone. *Science* **371**, 1148-1152 (2021).
6. Guidi, L. *et al.* Plankton networks driving carbon export in the oligotrophic ocean. *Nature* **532**, 465-470 (2016).
7. Cui, J. *et al.* Nanomagnetic encoding of shape-morphing micromachines. *Nature* **575**, 164-168, doi:10.1038/s41586-019-1713-2 (2019).
8. Lee, K. Y. *et al.* An autonomously swimming biohybrid fish designed with human cardiac biophysics. *Science* **375**, 639-647 (2022).
9. Yuk, H. *et al.* Hydraulic hydrogel actuators and robots optically and sonically camouflaged in water. *Nature Communications* **8**, 14230, doi:10.1038/ncomms14230 (2017).
10. Park, S.-J. *et al.* Phototactic guidance of a tissue-engineered soft-robotic ray. *Science* **353**, 158-162 (2016).
11. Li, G. *et al.* Self-powered soft robot in the Mariana Trench. *Nature* **591**, 66-71 (2021).
12. Picardi, G. *et al.* Bioinspired underwater legged robot for seabed exploration with low environmental disturbance. *Science Robotics* **5**, eaaz1012, doi:10.1126/scirobotics.aaz1012 (2020).
13. Yang, L. *et al.* Autonomous environment-adaptive microrobot swarm navigation enabled by deep learning-based real-time distribution planning. *Nature Machine Intelligence* **4**, 480-493, doi:10.1038/s42256-022-00482-8 (2022).
14. Kim, B. H. *et al.* Three-dimensional electronic microfliers inspired by wind-dispersed seeds. *Nature* **597**, 503-510, doi:10.1038/s41586-021-03847-y (2021).
15. Hu, W., Lum, G. Z., Mastrangeli, M. & Sitti, M. Small-scale soft-bodied robot with multimodal locomotion. *Nature* **554**, 81-85, doi:10.1038/nature25443 (2018).
16. Kim, Y., Yuk, H., Zhao, R., Chester, S. A. & Zhao, X. Printing ferromagnetic domains for untethered fast-transforming soft materials. *Nature* **558**, 274-279, doi:10.1038/s41586-018-0185-0 (2018).
17. Zhao, Y. *et al.* Soft phototactic swimmer based on self-sustained hydrogel oscillator. *Science Robotics* **4**, eaax7112, doi:10.1126/scirobotics.aax7112 (2019).
18. Palagi, S. *et al.* Structured light enables biomimetic swimming and versatile locomotion of photoresponsive soft microrobots. *Nat Mater* **15**, 647-653, doi:10.1038/nmat4569 (2016).
19. Wang, F. *et al.* Light control of droplets on photo-induced charged surfaces. *National Science Review*, nwac164, doi:10.1093/nsr/nwac164 (2022).
20. He, X. *et al.* Synthetic homeostatic materials with chemo-mechano-chemical self-regulation. *Nature* **487**, 214-218, doi:10.1038/nature11223 (2012).

21 Li, S. *et al.* Self-regulated non-reciprocal motions in single-material microstructures. *Nature* **605**, 76-83, doi:10.1038/s41586-022-04561-z (2022).
22 Qian, X. *et al.* Artificial phototropism for omnidirectional tracking and harvesting of light. *Nature Nanotechnology* **14**, 1048-1055, doi:10.1038/s41565-019-0562-3 (2019).
23 Ball, P. Animate materials. *MRS Bulletin* **46**, 553-559, doi:10.1557/s43577-021-00141-0 (2021).
24 Kaspar, C., Ravoo, B. J., van der Wiel, W. G., Wegner, S. V. & Pernice, W. H. P. The rise of intelligent matter. *Nature* **594**, 345-355, doi:10.1038/s41586-021-03453-y (2021).
25 Weitz, D. A. Soft materials evolution and revolution. *Nature Materials*, doi:10.1038/s41563-022-01356-5 (2022).
26 Camacho-Lopez, M., Finkelmann, H., Palffy-Muhoray, P. & Shelley, M. Fast liquid-crystal elastomer swims into the dark. *Nature Materials* **3**, 307-310, doi:10.1038/nmat1118 (2004).
27 Gelebart, A. H. *et al.* Making waves in a photoactive polymer film. *Nature* **546**, 632-636, doi:10.1038/nature22987 (2017).
28 Li, C. *et al.* Supramolecular-covalent hybrid polymers for light-activated mechanical actuation. *Nat Mater* **19**, 900-909, doi:10.1038/s41563-020-0707-7 (2020).
29 Bar-Cohen, Y. & Zhang, Q. Electroactive polymer actuators and sensors. *Mrs Bulletin* **33**, 173-181, doi:10.1557/mrs2008.42 (2008).
30 Christianson, C. *et al.* Jellyfish-Inspired Soft Robot Driven by Fluid Electrode Dielectric Organic Robotic Actuators. *Frontiers in Robotics and AI* **6** (2019).
31 Chen, X. *et al.* Relaxor ferroelectric polymer exhibits ultrahigh electromechanical coupling at low electric field. *Science* **375**, 1418-1422, doi:10.1126/science.abn0936 (2022).
32 Shi, Y. *et al.* A processable, high-performance dielectric elastomer and multilayering process. *Science* **377**, 228-232, doi:10.1126/science.abn0099 (2022).
33 Tang, L. *et al.* Poly(N-isopropylacrylamide)-based smart hydrogels: Design, properties and applications. *Progress in Materials Science* **115**, 100702, doi:https://doi.org/10.1016/j.pmatsci.2020.100702 (2021).
34 Zhao, Y. *et al.* Somatosensory actuator based on stretchable conductive photothermally responsive hydrogel. *Science Robotics* **6**, eabd5483 (2021).
35 Chen, C., Kuang, Y. & Hu, L. Challenges and opportunities for solar evaporation. *Joule* **3**, 683-718 (2019).
36 Guasto, J. S., Rusconi, R. & Stocker, R. Fluid Mechanics of Planktonic Microorganisms. *Annual Review of Fluid Mechanics* **44**, 373-400, doi:10.1146/annurev-fluid-120710-101156 (2011).
37 Gliwicz, M. Z. Predation and the evolution of vertical migration in zooplankton. *Nature* **320**, 746-748 (1986).
38 Gao, M., Zhu, L., Peh, C. K. & Ho, G. W. Solar absorber material and system designs for photothermal water vaporization towards clean water and energy production. *Energy & Environmental Science* **12**, 841-864 (2019).
39 Shin, B. *et al.* Hygrobot: A self-locomotive ratcheted actuator powered by environmental humidity. *Science Robotics* **3**, eaar2629 (2018).
40 Churchill, S. W. A comprehensive correlating equation for laminar, assisting, forced and free convection. *AIChE Journal* **23**, 10-16, doi:https://doi.org/10.1002/aic.690230103 (1977).
41 Wei, L., Lu, Y. & Wei, J. Mixed convection heat transfer from a particle in supercritical water.

Thermal Science **20**, 483-492, doi:10.2298/tsci131103038w (2016).